December 9, 2000

Spatial Structure of Simple Spiky Bursts at Microwave/Millimeter Wavelengths

M. R. Kundu, S. M. White,

Astronomy Department, University of Maryland, College Park, MD 20742

kundu,white@astro.umd.edu

K. Shibasaki

Nobeyama Radio Observatory, NAO, Minamisaku, Nagano 384-13, Japan

shibasak@nro.nao.ac.jp

T. Sakurai

National Astronomical Observatory, Mitaka, 181-8588 Japan

sakurai@solar.mtk.nao.ac.jp

V. V. Grechnev

Institute of Solar–Terrestrial Physics, Irkutsk, Russia

grechnev@iszf.irk.ru

ABSTRACT

We present the results of a study of spatial structure of sources of microwave and millimeter bursts with simple spiky time profiles at 17 and 34 GHz, similar to those found to be common at 3 mm wavelength. These bursts are of short duration, with fast 2 - 4 sec rise time to peak, followed by a rapid exponential decay. When mapped at high spatial resolution with the Nobeyama Radio Heliograph (NoRH), the radio images show direct evidence that the radio sources are compact bipolar loops: source sizes are less than $5''$ and 3 of the 5 events studied show closely–spaced oppositely–polarized components in the circular polarization maps. All 5 events are located directly over magnetic neutral lines in the photosphere. The soft X–ray behaviour is not entirely consistent with the

Neupert effect in these events, since all 5 events show a rise in the soft X–ray flux well before any nonthermal electrons are present in the corona, and the ratio of peak soft X–ray flux to peak radio 17 GHz flux may vary by many orders of magnitude from one event to the next. The abrupt time profiles of these events and their physical properties are consistent with a single–loop scenario in which magnetic energy release and acceleration of nonthermal electrons are confined to a compact localized region.

Subject headings: Sun: flares, radio radiation, corona

1. INTRODUCTION

Radio observations in principle provide a powerful technique for studying the spatial distribution of nonthermal electrons accelerated by solar flares through the gyrosynchrotron emission radiated by those electrons as they spiral along magnetic field lines in the solar corona (Dulk 1985; Bastian et al. 1998). Under suitable conditions, the nonthermal electrons "light up" the magnetic loops on which they reside, complementing soft X–ray and EUV observations of the loops containing hot thermal plasma. Appropriately designed radio telescopes can achieve high spatial resolution, high dynamic range images of such radio sources and in this paper we use the Nobeyama Radio Heliograph (NoRH) to investigate the spatial structure of a particular class of radio bursts.

Over the past several years, we have demonstrated with the Berkeley–Illinois–Maryland Association (BIMA) interferometer that millimeter wavelength observations can be used to study the production of electrons with energies of order 1 MeV and higher in "ordinary" solar flares. This is because the gyrosynchrotron emission of relatively small numbers of nonthermal MeV-energy electrons can be detected rather easily with the millimeter-wavelength interferometers. The typical range of magnetic field strengths in the corona requires that millimeter emission be at high harmonics of the electron gyrofrequency, and since nonrelativistic electrons have low emissivity at such high harmonics the observed millimeter emission must be dominated by the contribution of MeV energy electrons (White & Kundu 1992). White (1994) reported a striking morphology in the time profiles of the impulsive phase of millimeter bursts. The first event in this category reported by White et al. (1992) showed a linear rise to a sharp peak in 6 seconds, followed by an immediate decay of exponential form with a decay constant of 18 seconds. Since then, a remarkable similarity has been found in the time profiles of emission associated with the impulsive onsets of a good fraction of all flares. In a large fraction of flares studied until 1995 (50% of the 50 events in which the impulsive phase was well-observed by BIMA), the impulsive phase emission at millimeter wavelengths consists of a rapid rise ($\sim$ 5 seconds) linear in time to a sharp peak, followed by an exponential decay with a decay constant of order 45 seconds. By contrast, the .3 - 1 MeV bremsstrahlung from electrons in the same energy range tends to show impulsive spikes on the same timescale with more symmetric rise and decay profiles. This time profile is not restricted to small flares alone: it has been seen in events ranging in GOES class from less than B3 up to M5. The corresponding range in millimeter flux at the peak is about a factor of over 50, from less than 3 sfu up to 15 sfu.

This linear rise-exponential decay time profile common to impulsive millimeter emission is not generally shared by the microwave emission nor by the hard X–ray emission in the same events. In general the microwave profiles have a more gradual initial rise and a more rounded peak than does the millimeter profile. Hard X-rays in the 25 - 100 keV range also often show time profiles quite different from the corresponding millimeter emission (Kundu et al. 1994). Since we interpret the nonthermal impulsive-phase millimeter emission as a diagnostic of the MeV-energy electrons, this means that they have a property not shared by the lower-energy electrons responsible for the hard X-rays (typically 25 - 100 keV) and microwaves (probably 100 - 500 keV). There is also some evidence that the spectral energy distribution of the millimeter–emitting electrons differs from that of the hard X–ray-emitting electrons.

It seems that for these events the production of MeV-energy electrons follows a very similar pattern. The simplest interpretation of the morphology seems to be that the electrons are accelerated, or somehow injected into a coronal loop, on a timescale of several seconds (the linear rise), but acceleration then ceases abruptly and the number of electrons in the corona decreases exponentially. As wave-particle processes scatter electrons into the loss cone and they precipitate into the corona, the similarity in the rise time and decay time among a large number of events would then impose strong constraints on the mechanism of acceleration and the conditions in which it occurs.

Since essentially the same electrons that radiate at 86 GHz should also dominate the emission at 34 GHz, which is generally on the optically–thin (high–frequency) side of the spectral peak, we expect that they should be commonly observed by the Nobeyama radioheliograph (NoRH). Inspection of the NoRH correlation plots (effectively time profiles of the small–spatial–scale flux at 17 and 34 GHz) shows that indeed bursts of this type are commonly detected. In this paper we report on the source structures of five spiky simple bursts observed at both 17 and 34 GHz by NoRH. We use superresolution techniques in order to exploit fully the spatial resolution available in the NoRH data.

2. OBSERVATIONS

The Nobeyama Radio Heliograph (Nakajima et al. 1994) consists of 84 antennas in a T–shaped array. It observes the full solar disk in two circular polarizations at 17 GHz and one linear polarization at 34 GHz, with subsecond time resolution for burst events. The data presented here were processed in the NRAO software package AIPS using techniques developed by T. S. Bastian, K. Shibasaki and S. Enome and partially described by Nindos et al. (1999). Since in this study our prime goal is to achieve optimal spatial resolution, the final images were made using uniform weighting, cleaned, self–calibrated and then restored with beam sizes of $10''$ or $12''$ at 17 GHz and $6''$ or $8''$ at 34 GHz. The resulting dynamic range in the images is as high as 10^3, so weak features should be readily visible. The basic details of the events, including locations, GOES classes, 17 and 34 GHz peak fluxes and 17 and 34 GHz deconvolved sizes at the times of the peaks, are given in Table 1. The sizes are determined by treating the source in the image as the convolution of the true source (assumed to be a two–dimensional Gaussian in shape) with the Gaussian used for the restoring beam in the images: this can be done as long as the signal–to–noise is adequate. The formal uncertainties in the size measurements are in all cases much less than $1''$. Figures 1-3 and 5-6 use a common format to present the events, including preflare images at 17 GHz (in most cases there was no significant preflare emission at 34 GHz), flare images at 17 and 34 GHz, and time profiles at 17 and 34 GHz and in soft X–rays. Longitudinal photospheric magnetograms from the Michelson Doppler Imager (MDI) on the Solar and Heliospheric Observatory spacecraft (SOHO) or from the Kitt Peak National Observatory spectromagnetograph are shown for context information. We estimate that the accuracy of the overlays of the 17 GHz radio flare images on the magnetograms is not generally better than $5''$. The maximum longitudinal magnetic field strength observed in each of the regions shown in the figures is given in Table 1.

2.1. Event of April 1, 1997

This burst (Figure 1) is the second longest of the events with a duration of approximately 60 s. The rise time is 7 s and the full–width at half maximum (FWHM) is 13 s. The time profiles are very similar at 17 and 34 GHz. The event occurred in the middle of an active region with no prominent peaks prior to the flare: the peak preflare brightness temperature is only 18000 K and there is only very weak polarization in the preflare stage, indicating that coronal magnetic fields were relatively weak in this region. The flare source is located just to the northwest of the preflare peak in the 17 GHz I and V maps. This event is moderately circularly polarized at 17 GHz (just over 10%), but appears to be unipolar in these data. The burst is located right at a neutral line in the photospheric magnetogram. Careful inspection of the 17 GHz V contours at the flare peak shows that they are not symmetric, with the south–eastern side of the source declining more abruptly than the north–western side. This would be consistent with the observed radio polarization arising predominantly from the positive polarity (north–west) side of the neutral line. The deconvolved sizes of the flare source are given in Table 1: approximately $4''$ at 17 GHz and slightly smaller at 34 GHz (significantly less than the nominal beam size of the NoRH data in both cases). The source size for this event does not change significantly as it decays. Note that the impulsive phase of the radio emission begins after the onset of the rise in soft X–rays.

2.2. Event of May 6, 1998

With a rise time of 1 s and a FWHM of just 2 s, this burst is one of the most impulsive events ever seen at high microwave frequencies. Emission effectively ceases completely within 5 s of onset. The time profiles are similar at both 17 and 34 GHz. The flare producing region is near the south–west limb in a region with a very strong gyroresonance source prior to the event (peak brightness temperature of 2×10^5 K, 25% negatively circularly polarized). At high resolution (Figure 2) this preflare gyroresonance source is resolved into two discrete components, both negatively polarized. The radio burst appears at the northern edge of the more northerly of the two preflare gyroresonance sources, and results in a brief period when positive circular polarization can be detected at this location. The magnetogram does suggest the presence of positive magnetic polarity in this location, although because the event is at the limb the actual magnetic topology is not clear. The morphology of the circular polarization map at this time, with a steep gradient in circularly polarized flux at the "radio neutral line", is characteristic of a bipolar source that is not fully resolved by the observations, and therefore we believe that the true degree of circular polarization at 17 GHz was higher than is apparent in these images, where the peak is around 10%. Deconvolved source sizes at the peak of the event are again of order $4''$ at 17 GHz and $3''$ at 34 GHz, expanding to $8''$ and $5''$ respectively as the source decays. Note that this is also the only one of the five events in which the 34 GHz flux exceeds the 17 GHz flux: the spectrum is rising from 17 to 34 GHz, implying high coronal magnetic fields in the source. Again, the impulsive phase of the radio emission begins after the onset of the rise in soft X–rays.

2.3. Event of June 13, 1998

This event occurred in an active region near the east limb. Its peak was at 04:18:36 UT. The preflare 17 GHz images show a moderately strong gyroresonance source (Figure 3), and the flare source is located right at the radio neutral line apparent in the preflare images. The flare radio source itself is bipolar and polarized at about 5%, with an orientation and location exactly matching that of the preflare neutral line. The photospheric magnetogram shows a dominantly negative polarity in the region with a shape consistent with that of the negatively–polarized emisison in the preflare 17 GHz V map. There is positive magnetic flux to the northwest and the orientation of the photospheric neutral line is consistent with that of the radio neutral line both prior to and during the flare. The burst has a rise time of 6 s and a FWHM of 7 s. At its peak the deconvolved size at 17 GHz is $4''.2 \times 2''.5$, which expands to $8'' \times 5''$ as the source decays.

This event has been imaged by the Hard X–ray Telescope (HXT) in the high–energy H band (53-93 keV), as well as in the M2 (33-53 keV), M1 (23-33 keV) and L (14-23 keV) bands. Figure 4 shows the hard X–ray (HXR) time profiles in the various bands along with 17 and 34 GHz NoRH time profiles. As expected, there is close similarity in these time profiles, with the peaks appearing at the same time. Note also that the impulsive HXR burst is of the same duration as the 17 and 34 GHz bursts. Since the hard X–rays represent precipitating electrons while the microwave emission includes trapped electrons, the implication is that relatively little trapping of nonthermal electrons occurred in this loop, which is consistent with the loop being small and implies that the magnetic field may not have varied much along the loop. The HXT images show a compact source consistent in size with the radio source: its nominal position is $15''$ away from the radio source, but we believe that this positional offset is instrumental and that the HXR source is in fact coincident with the radio source. Unfortunately, we do not have any SXR images at the time of the flare, because Yohkoh-SXT was looking at a different region. However, we have pre- and post-flare SXR images, which show large loop-like structures in the flaring region. The 17 and 34 GHz sources as well as the HXR source are located near one end (or foot point) of the large SXR loop-like structure.

2.4. Event of July 13, 1998

This burst has a rise time of 5 s and a FWHM of 7 s; the decay phase shows two stages, an initial sharp drop followed by a more gradual decline starting at 03:38:16 UT. The event occurs in the trailing part of a region showing a bright but weakly polarized gyroresonance source in the preflare 17 GHz image, with a morphology in which the peak in the circularly polarized image is not coincident with the peak in the total intensity image (Figure 5). The flare images again show a compact morphology in the 17 and 34 GHz total intensity images and a bipolar morphology in the 17 GHz V map, with positive polarity being stronger. The peak degree of polarization in the 17 GHz images is around 10%. The magnetogram indicates that the radio burst lies right over a photospheric neutral line, and the radio neutral line has an orientation consistent with the photospheric neutral line. In this event the deconvolved sources appear to be quite highly elongated: $5'' \times 2''$ at 17 GHz and $5'' \times 1''$ at 34 GHz, although the elongation is apparently parallel to the radio neutral line rather than orthogonal to it as one would expect for a bipolar loop. As the source decays the size expands slightly to $6'' \times 3''$ at 17 GHz.

2.5. Event of July 30, 1999

This event is also extremely brief, with a rise time of 2 s and a FWHM of 4 s. It occurs near the leading spot in a complex active region in the north–east of the solar disk, which has quite a strong gyroresonance source in the preflare images at 17 GHz (Figure 6). Because of the nearby presence of this strong gyroresonance source image analysis of the flare itself is difficult and the true deconvolved size of the flare source is difficult to determine in the 17 GHz I map. The 17 GHz total intensity image is clearly elongated at the time of the flare peak, but the 17 GHz V map shows that there are two sources present producing the east–west elongation, one coincident with the preflare gyroresonance source and the other just $18''$ to the east of it. The V flux of the gyroresonance source does not appear to change during the flare, and the peak in the 17 GHz I flare image lies between the two sources in the V map. We are able to do a careful coalignment of the 17 and 34 GHz images for this event thanks to the presence of nonflare emission elsewhere in the active region that is visible at both frequencies. Interestingly, the 34 GHz flare source is coincident with the 17 GHz flare peak and also lies between the two sources in the V map, rather than being coincident with the eastern source in the 17 GHz V map that was not present prior to the flare. Hence this appears to be an event that is only very weakly polarized at the location of the 17 GHz I peak (reaching only about 10% at the location of the V peak) and where the 34 GHz source does not obviously lie at a loop footpoint.

Hard X–ray emission from this event was detected both by Yohkoh/HXT and by CGRO/BATSE. Both instruments show a very brief burst of hard X–rays, with a FWHM of just 3 seconds in the 25 – 50 keV channel of BATSE, consistent with the radio time profile. The position and size of the hard X–ray source in the HXT images is consistent with the radio position, but we do not have a coalignment accurate at the arcsecond level that would allow us to identify the hard X–rays with a particular radio feature.

The photospheric magnetogram again shows a neutral line right under the 17 GHz flare source produced by a finger of negative flux intruding into the positive polarity associated with the leading spot in the region. Inspection of a sequence of MDI magnetograms shows negative flux from this finger moving westwards until it becomes surrounded by positive polarity and eventually disappears.

3. TRAP MODELS

In this section we investigate the relationship of the hard X-ray and radio time profiles using a simple trap model. At the simplest level, we can regard the acceleration of nonthermal electrons as a process that injects these electrons onto magnetic field lines at a time–dependent rate $f_I(t)$ (electrons per second). If the magnetic field varies along the field lines on which the electrons are released, then there is a critical pitch angle, called the loss cone angle, such that electrons with smaller pitch angles are not reflected by the increasing magnetic field as they approach the footpoints. Some fraction of these electrons Q are injected with pitch angles lying in the loss cone, and unless strong pitch angle scattering is present these electrons will precipitate on their first approach to a footpoint of the loop. The remaining fraction $1 - Q$ of the electrons is injected with pitch angles outside the loss cone and they will remain trapped in the solar corona unless pitch angle scattering takes place. The parameter Q depends on the geometry of the loop on which the nonthermal electons are injected, and on the nature of the pitch angle distribution of the accelerated electrons, so knowledge of Q would be a valuable constraint on acceleration mechanisms.

The effects of pitch-angle scattering and energy loss on the trapped population can be modelled simply by adopting a loss time τ such that the rate of change of the number of trapped electrons $n_T(t)$ is governed by an equation

$$\frac{\mathrm{d}}{\mathrm{dt}}\, n_T(t) \;=\; (1 \,-\, Q)\, f_I(t) \;-\; \frac{n_T(t)}{\tau} \tag{1}$$

with the solution $n_T(t) \;=\; (1 \,-\, Q)\, N_T(t)$ where

$$N_T(t) \;=\; \int_{-\infty}^{t} \exp\left[-\frac{(t \,-\, t')}{\tau}\right]\; f_I(t')\; \mathrm{dt} \tag{2}$$

For compact loops of arcsecond dimensions such as those inferred for the events discussed in this paper, the bounce times for radio–emitting electrons are of order tens of milliseconds and thus are averaged over in the data available, which have a time resolution of 1 second. Nonthermal electrons will radiate gyrosynchrotron emission at radio wavelengths as long as they are moving through the corona. Thus both the trapped and the injected electrons will produce radio emission. This suggests that one can decompose the radio light curve as the sum of two components: one proportional to the injected electron rate, which can be represented by a hard X–ray time profile, and the other proportional to the time profile of the number of trapped electrons, represented by (2) calculated using the same injection function, i.e.,

$$S(t) \; \propto \; q \, f_I(t) \; + \; (1 \, - \, q) \, N_T(t) \tag{3}$$

This is similar to the rate of hard X–ray production by a combination of trapped and directly precipitating electrons (Aschwanden 1998). Figures 7 & 8 show the results of such a determination for the two events we discuss for which hard X–ray data exist to serve as injection functions: 1998 June 13 (Fig. 7) and 1999 July 30 (Fig. 8). The radio and hard X–ray light curves are normalized to a peak of unity: for a given decay time τ the trapped population time dependence is obtained from (2) and then the best-fit values for τ and q are obtained by minimizing the difference between the model light curve and the observed radio time profile, and interpreting the ratio of the trapped and untrapped components as $(1 \, - \, q)/q$. This is carried out separately for both 17 and 34 GHz light curves.

For the 1998 June 13 event we find the same value of q for both frequencies but very different decay times: 12.9 s at 17 GHz but 35 s at 34 GHz. For 1999 July 30 we find different parameters at 17 and 34 GHz: τ = 5.0 s and q = 0.24 at 17 GHz, τ = 13.9 s and q = 0.10 at 34 GHz. In addition, the 17 GHz light curve rises before the hard X-ray light curve, and this component cannot be accounted for with either the directly injected or trapped components. We have not attempted to determine uncertainties in these values for reasons discussed below. We note that both τ and q are largely determined by the decay phase of the radio light curve when the flux levels may be low, leading to large uncertainties for weak events.

The value of τ determined from this analysis presumably represents a mean decay time for the electrons that dominate the radio emission at the frequency used. The gyrosynchrotron emissivity η has a relatively broad energy dependence and we expect the same electrons to dominate at all high optically–thin frequencies, so a large difference between τ at 17 and 34 GHz is not consistent with the starting assumptions if the two frequencies are both on the high–frequency side of the spectral peak as is the case for the 1998 June 13 event. For the 1999 July 30 event the radio spectral peak probably lies between 17 and 34 GHz, so the 17 GHz emission may be optically thick and this can explain the difference in

τ at the two frequencies.

The parameter q is more difficult to interpret. The number of trapped electrons (2) actually refers to a single energy only: both τ and the injection function f_I are energy–dependent, and the gyrosynchrotron emission mechanism that produces the radio emission is also energy dependent. Strictly, (1) also includes a source term due to energy diffusion, which we have ignored. The gyrosynchrotron emissivity also depends on the pitch angle distribution (Φ), which by definition is different for the directly precipitating and trapped populations. An additional parameter is required to account for the fact that $f_I(t)$ is an injection rate, whereas the radio flux is proportional to the number of electrons in the loop: to determine the number of electrons in the loop but on their way directly to the footpoints we use the injection rate times the transit time across the loop at the energy of interest ($L/2v$ for a loop of length L and particle of velocity v, ignoring the pitch angle dependence of the transit time and assuming an injection point halfway along the loop). This parameter does not enter the calculation of the hard X–ray production (Aschwanden 1998). Thus the dependence of the radio flux on the injection function is actually of the form

$$S(t) \;=\; Q \int dE\, \eta(E,\Phi_I)\, f_I(E,t)\, \frac{L}{2v} \;+\; (1\,-\,Q) \int dE\, \eta(E,\Phi_T)\, N_T(E,\tau_E,t) \qquad (4)$$

In addition, the electrons which produce the radio emission generally appear to be a population different from those which produce the hard X–rays (Dennis 1985; Lim et al. 1992; Kundu et al. 1994; Silva et al. 1997; Vilmer & Trottet 1997; Raulin et al. 1999), so in general it is not the case that, e.g., 50 keV hard X–rays represent the appropriate injection function for the radio–emitting electrons (to be specific, there are events in which the 50 keV hard X–rays last longer than the nonthermal radio emission, which cannot occur in the standard trap model). The additional unknown parameters L, Φ_I, Φ_T and the energy dependences of τ, f_I and n_T mean that we cannot determine the physically interesting parameter Q from the observable parameter q without additional information: they could easily differ by large factors.

4. DISCUSSION

We have studied the spatial source structures of microwave and millimeter simple spiky bursts with the NoRH at 17 and 34 GHz. These bursts are of short duration, with fast 2 - 10 sec rise times to the peak, followed by a rapid exponential decay. These bursts can be of any intensity, from 1 sfu to 10's of sfu; they are often strongly polarized ($\simeq$ 50%), and they have similar properties regardless of the nature of the active region in which these bursts originate. The bursts seem to originate in compact sources that have sizes typically no larger than $5''$ at 17 GHz and $4''$ at 34 GHz. Both the radio images and the photospheric magnetograms provide direct evidence that these compact sources are simple bipolar loops. Three of the five events are bipolar in the V maps at 17 GHz, and in each case it appears that oppositely polarized footpoints are separated by less than $5''$. In every one of the 5 events the radio source is found to lie over a magnetic neutral line in the photosphere, to within the accuracy of the overlays, and furthermore the orientations of the photospheric magnetic neutral lines are consistent with the orientations inferred from the 17 GHz V maps. We have no evidence here that any of these events involve an interaction between the compact loop and a larger loop near one foot point that triggers the flare, as in the class of events studied by Hanaoka (Hanaoka 1997, 1999). Hanaoka's analysis was based upon several 17 GHz flaring sources, which were selected to be bipolar with the two foot points of opposite polarity being well separated; those flares were more intense and of much longer duration than the bursts discussed in this paper. Nishio et al. (1997) studied 14 impulsive flares in order to understand their magnetic field configurations and also found that two loops were commonly present in the 17 GHz emission. Those events, while still impulsive, were generally of much longer duration than the events discussed here, so there is no conflict with this study. Other radio images of flares have shown two well–separated footpoints at high frequencies where the source is likely to be optically thin (Shevgaonkar & Kundu 1985; Alissandrakis et al. 1993; Nindos et al. 2000) and fully–outlined loops at low frequencies where the source is optically thick (Dulk et al. 1986; Bastian & Kiplinger 1991; Bastian & Gary 1992; Kucera et al. 1994; Wang et al. 1994; Nindos et al. 2000). Shimizu (1997) has proposed emerging flux of opposite polarity interacting with pre-existing flux as a possible cause of active region transient brightening(ARTB). This explanation does not seem to be appropriate for our case either. In our case, the simple bipolar loop flares up and produces weak simple spiky bursts at microwave and millimeter wavelengths.

The short duration, simple spiky time profiles and compact bipolar loop morphology of these bursts are consistent with a scenario in which the radio–emitting nonthermal electrons are produced/accelerated in a compact simple bipolar loop. These accelerated electrons must be produced in the compact loop on a time scale of several seconds following some instability; then the acceleration ceases abruptly and the number of electrons in the loop decreases exponentially (e.g., White 1994). The exact mechanism that does this is not known, although there are several possibilities. For example, wave-particle processes may scatter the electrons into the loss cone and they precipitate along field lines into the foot points. The inferred loop sizes of order 3000 km correspond to very short electron propagation times (tens of milliseconds), so that electrons can experience many bounce periods during the observed short durations of the bursts.

Another property shared by all five events is that the soft X–ray rise associated with the flare begins prior to the impulsive rise of the radio emission. This suggests that some preflare heating takes place and that acceleration of electrons to nonthermal energies is not initiated until later in the events. Since no nonthermal electrons are present during the initial soft X–ray rise, these events are not consistent with a scenario in which all the soft X–rays are produced by chromospheric material heated to coronal temperatures by precipitating nonthermal electrons. Thus these events are not strictly consistent with the "Neupert effect" (Neupert 1968). It is also apparent from Table 1 that there is little correlation between the GOES soft X–ray class of an event and its peak 17 GHz flux: the events on 1998 June 13 and 1998 July 13 reached soft X–ray fluxes that differed by a factor of 1000, yet their 17 GHz fluxes differed only by a factor of 2. Such a difference could in principle by explained by the fact that gyrosynchrotron radio emission is a strong function of magnetic field strength (Dulk 1985), whereas soft X–ray emission has no dependence on magnetic fields. On the other hand, the magnetic field in the radio source should be linearly proportional to the frequency at which the radio spectrum of the burst peaks (Dulk & Marsh 1982), and for all these events the spectral peak is probably in the range 15 – 30 GHz based on the 17 and 34 GHz fluxes, while the photospheric data show similar line–of–sight maximum field strengths in the flare regions (Table 1). Consequently we would not expect there to be much variation in magnetic field strength between these events, and the wide spread in the ratio of soft X–ray to radio flux remains unexplained.

5. CONCLUSIONS

We have presented high–resolution radio imaging of nonthermal electrons in five events selected on the basis of their time profiles at 17 and 34 GHz. They exhibit a linear rise time of less than 10 s and an exponential decay of time constant less than 15 s, which is similar to a time profile shape found to be common at 3 mm wavelength. These bursts can be of any intensity, from $\sim$ 1 sfu to 10s of sfu; they are often strongly polarized ($\gtrsim$ 50%). When mapped at high spatial resolution with the Nobeyama Radio Heliograph (NoRH), direct evidence that the radio sources are compact bipolar loops is seen: three of the five events show bipolar sources in the circular polarization maps. We interpret these as the oppositely polarized footpoints of loops whose size is less than $5''$. Every one of the events lies over a neutral line in the photospheric magnetogram and the bipolar V sources have orientations consistent with the footpoints of a loop straddling the neutral line. Such small source sizes are consistent with the short durations of the events. We interpret them as simple single–

loop flares, although of course we cannot rule out the possibility that there is interaction on even smaller scales for which our available spatial resolution is inadequate. The soft X–ray behaviour is not entirely consistent with the Neupert effect in these events.

Acknowledgments

This research at the University of Maryland was carried out with support from NSF grants ATM 99-09809 and INT 98–19917, and NASA grants NAG 5-7370, NAG 5-8192 and NAG 5-7901. We thank Alexander Nindos for valuable comments and advice, and Helen Coffey and Susan Wahl for providing RSTN data. We thank the SOHO/MDI team and the National Solar Observatory for making their magnetogram data freely available.

REFERENCES

Alissandrakis, C. E., Nindos, A., & Kundu, M. R. 1993, Solar Phys., 147, 343

Aschwanden, M. J. 1998, ApJ, 502, 455

Bastian, T. S., Benz, A. O., & Gary, D. E. 1998, ARA&A, 36, 131

Bastian, T. S. & Gary, D. E. 1992, Solar Phys., 139, 357

Bastian, T. S. & Kiplinger, A. 1991, in Max '91 Workshop 3: Max '91/SMM Solar Flares, Observations and Theory, ed. R. Winglee & A. Kiplinger (Boulder: NOAA/SEL), 153

Dennis, B. R. 1985, Solar Phys., 100, 465

Dulk, G. A. 1985, ARA&A, 23, 169

Dulk, G. A., Bastian, T. S., & Kane, S. R. 1986, ApJ, 300, 438

Dulk, G. A. & Marsh, K. A. 1982, ApJ, 259, 350

Hanaoka, Y. 1997, Solar Phys., 173, 319

—. 1999, PASJ, 51, 483

Kucera, T. A., Dulk, G. A., , Gary, D. E., & Bastian, T. S. 1994, ApJ, 433, 875

Kundu, M. R., White, S. M., Gopalswamy, N., & Lim, J. 1994, ApJS, 90, 599

Lim, J., White, S. M., Kundu, M. R., & Gary, D. E. 1992, Solar Phys., 140, 343

Nakajima, H., Nishio, M., Enome, S., Shibasaki, K., Takano, T., Hanaoka, Y., Torii, C., Sekiguchi, H., & 9 others. 1994, Proc. IEEE, 82, 705

Neupert, W. M. 1968, ApJL, 153, L59

Nindos, A., Kundu, M. R., White, S. M., Gary, D. E., Shibasaki, K., & Dere, K. P. 1999, ApJ, 527, 415

Nindos, A., White, S. M., Kundu, M. R., & Gary, D. E. 2000, ApJ, 533, 1053

Nishio, M., Yaji, K., Kosugi, T., Nakajima, H., & Sakurai, T. 1997, ApJ, 489, 976

Raulin, J., White, S. M., Kundu, M. R., Silva, A. R., & Shibasaki, K. 1999, ApJ, 522, 547

Shevgaonkar, R. K. & Kundu, M. R. 1985, ApJ, 292, 733

Shimizu, T. 1997, Ph.D. thesis (University of Tokyo)

Silva, A. V. L., Gary, D. E., White, S. M., Lin, R. P., & de Pater, I. 1997, Solar Phys., 175, 157

Vilmer, N. & Trottet, G. 1997, in Coronal Physics from Radio and Space Observations, ed. G. Trottet (Berlin: Springer), 28

Wang, H., Gary, D. E., Lim, J., & Schwartz, R. A. 1994, ApJ, 433, 379

White, S. M. 1994, in High Energy Solar Phenomena: A New Era of Spacecraft Measurements, ed. J. Ryan & W. T. Vestrand (New York: AIP Conf. Proc. **294**), 199

White, S. M. & Kundu, M. R. 1992, Solar Phys., 141, 347

White, S. M., Kundu, M. R., Bastian, T. S., Gary, D. E., Hurford, G. J., Kucera, T., & Bieging, J. H. 1992, ApJ, 384, 656

Table 1. Flare source data.

Date	Time (UT)	Location (deg)	GOES class	Max B (G)	17 GHz flux (sfu)	34 GHz flux (sfu)	17 GHz size ($''$)	34 GHz size ($''$)
1997 Apr 01	01:48:50	S26E24	A1	1030	18	12	4.4×2.8	3.7×1.4
1998 May 06	23:16:36	S14W72	B2	820	14	52	3.9×3.4	3.3×2.1
1998 Jun 13	04:18:36	S27E54	M2	870	75	37	4.4×2.5	3.0×2.2
1998 Jul 13	03:38:10	S22E33	A2	640	33	28	5.5×2.2	5.1×1.2
1999 Jul 30	22:58:09	N24E38	A1	1180	18	9	10×5	5.3×3.1

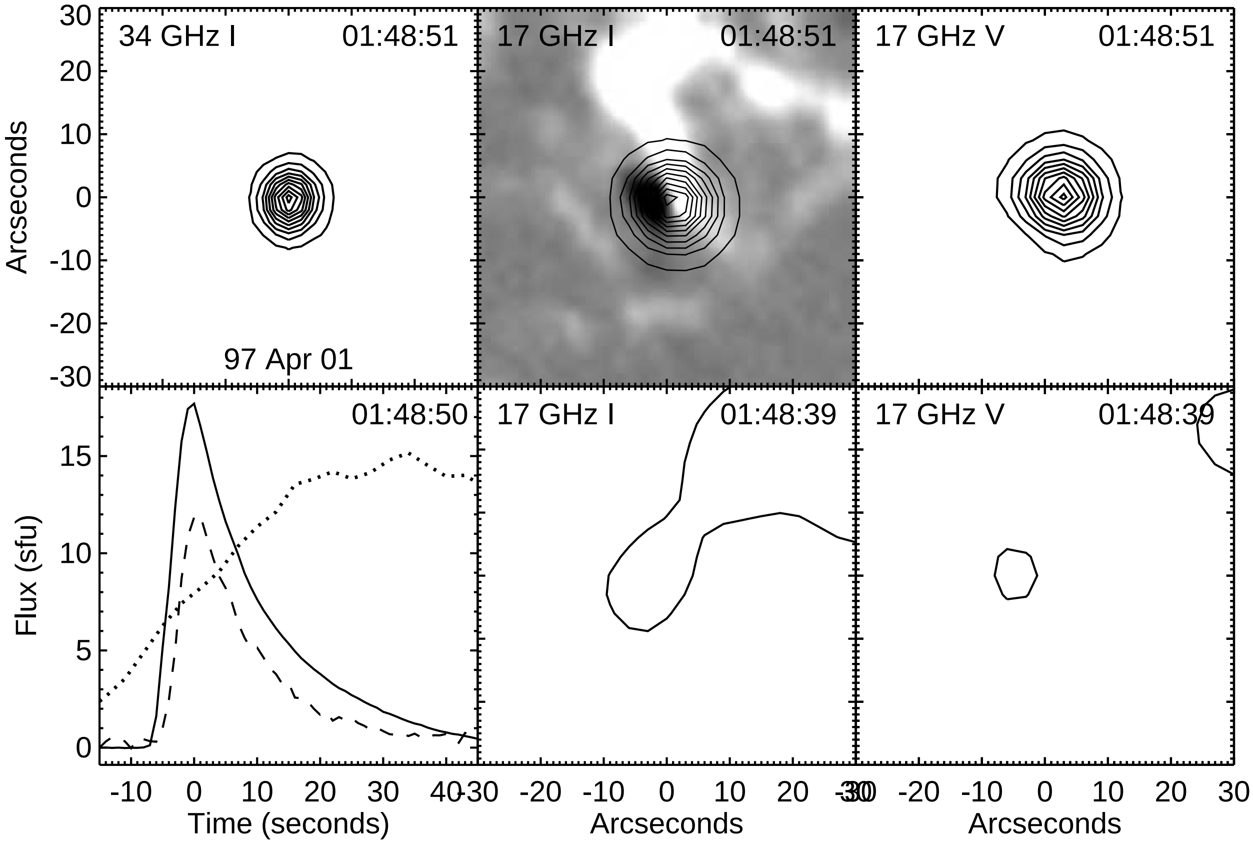

Fig. 1.— NoRH time profiles and images of the flare at 01:48:50 UT on 1997 April 1. The three upper panels show images at the peak of the flare at 34 GHz in total intensity in the left panel, at 17 GHz in total intensity in the middle panel and at 17 GHz in circularly polarized intensity in the right panel. The greyscale image in the upper middle panel is a SOHO/MDI longitudinal magnetogram taken at 01:35:04 UT, with a linear display of magnetic field strength saturating at $\pm$ 400 G. The lower left panel shows 1 second resolution time profiles of the radio flux at 17 GHz (solid line) and 34 GHz (dashed line) and a 3 second resolution profile of the soft X–ray flux measured by the GOES satellite in the 1.5 – 10 keV channel (dotted line, scaled arbitrarily). The time range plotted spans from 15 seconds prior to the 17 GHz peak to 45 seconds after the 17 GHz peak. The lower middle panel shows a preflare image of the total intensity at 17 GHz while the lower right panel shows a preflare image of the circularly polarized intensity at 17 GHz. Contours are plotted at 5, 15, 25, ..., 95% of the respective peaks in the 34 (2.4×10^6 K) and 17 GHz (5.5×10^6 K) total intensity flare images, and at degrees of polarization of 0.5, 1.5, 2.5, ..., 9.5% in the 17 GHz circular polarization image (with positive polarity plotted with a solid line and negative polarity with a dashed line). In the preflare images contours in the 17 GHz total intensity map are plotted at brightness temperatures of 15000, 25000, ..., 105000 K, and in the 17 GHz circularly polarized map contours are plotted at $\pm$2500, $\pm$7500, $\pm$12500, ..., $\pm$47500 K.

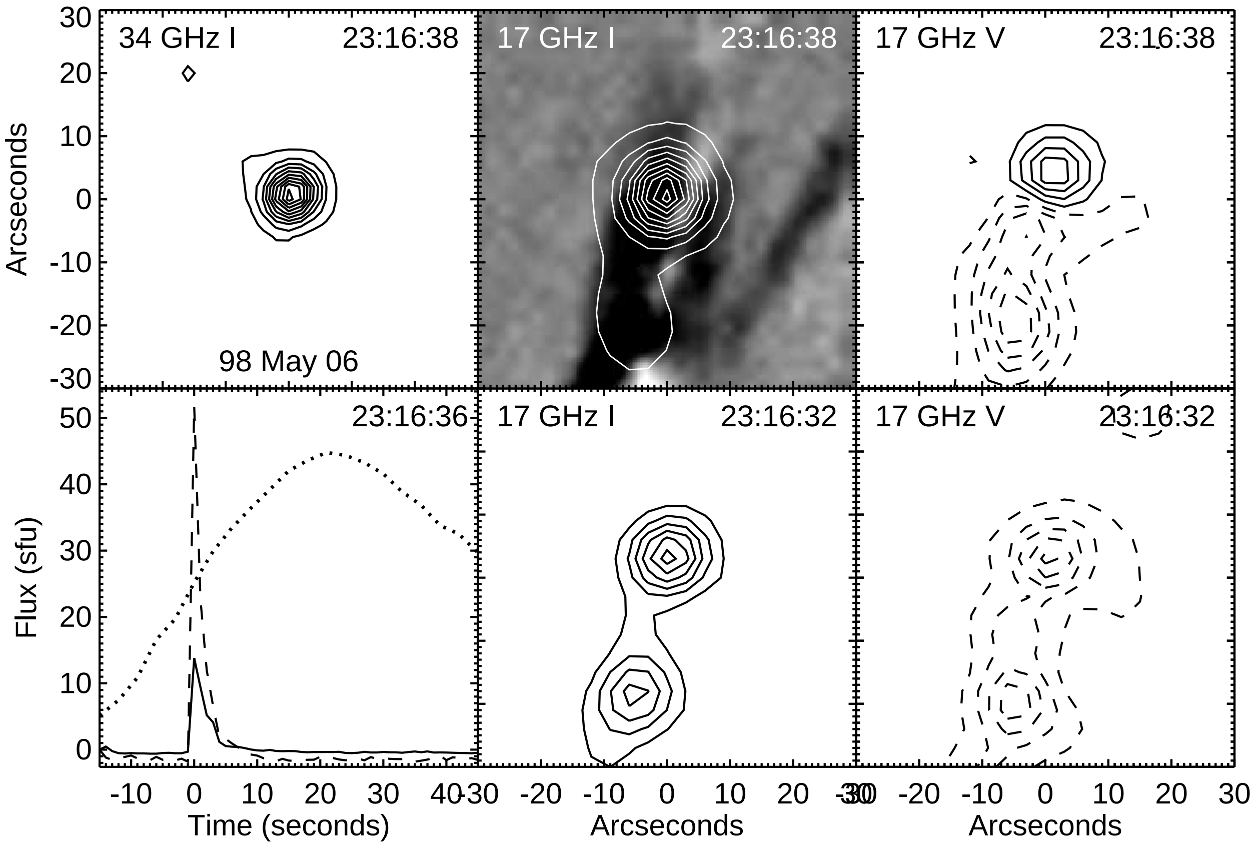

Fig. 2.— NoRH time profiles and images of the flare at 23:16:36 UT on 1998 May 6. The format is identical to that of Fig. 1, with the peak brightness temperatures being 4.7×10^6 K at 34 GHz and 4.3×10^6 K at 17 GHz. In the preflare images, contours are plotted at brightness temperatures of 150000, 250000, ..., 650000 K in the total intensity map and ±25000, ±75000, ±125000, ..., ±225000 K in the circularly polarized map. The SOHO/MDI magnetogram was taken at 22:23:04 UT.

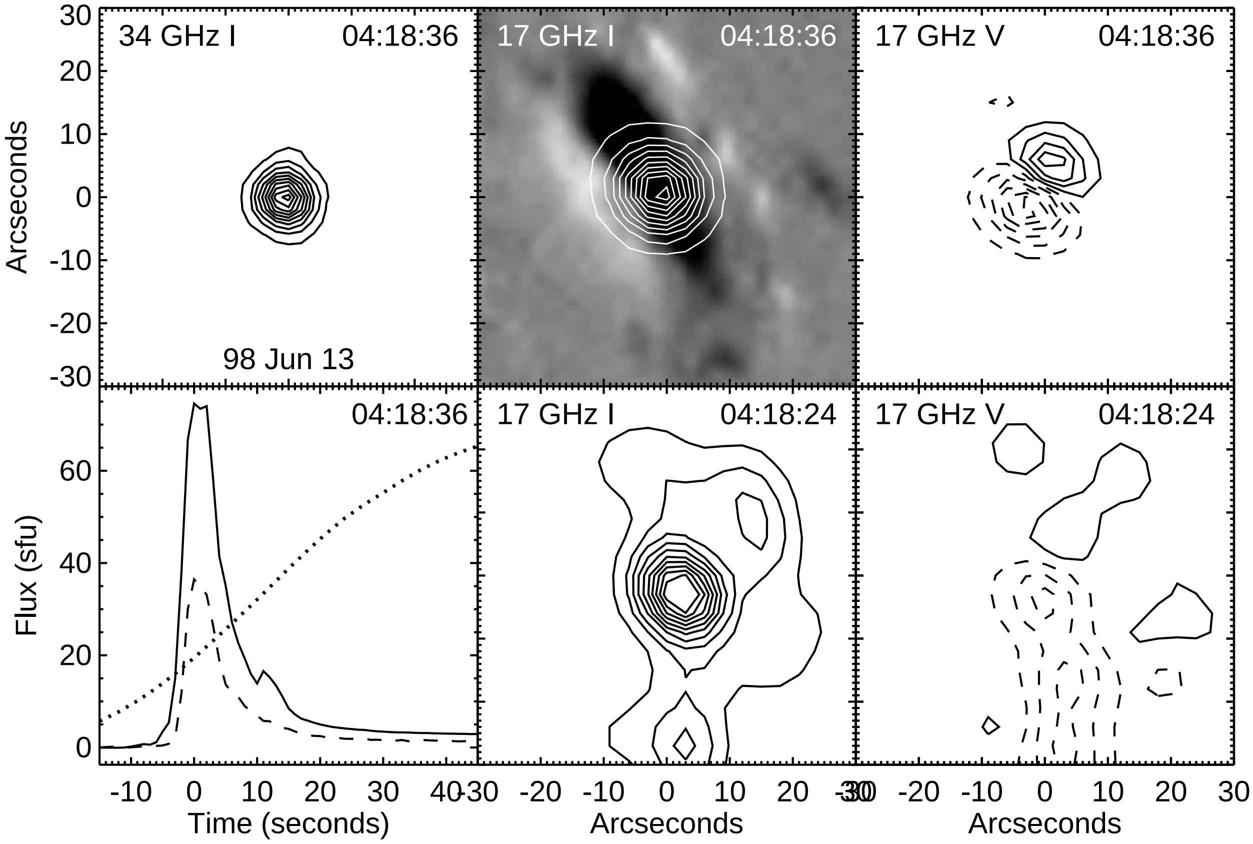

Fig. 3.— NoRH time profiles and images of the flare at 04:18:36 UT on 1998 June 13. The format is identical to that of Fig. 1, with the peak brightness temperatures being 8.4×10^6 K at 34 GHz and 2.8×10^7 K at 17 GHz. In the preflare images, contours are plotted at brightness temperatures of 30000, 50000, ..., 130000 K in the total intensity map and ±5000, ±15000, ±25000 K in the circularly polarized map. The SOHO/MDI magnetogram was taken at 04:48:04 UT.

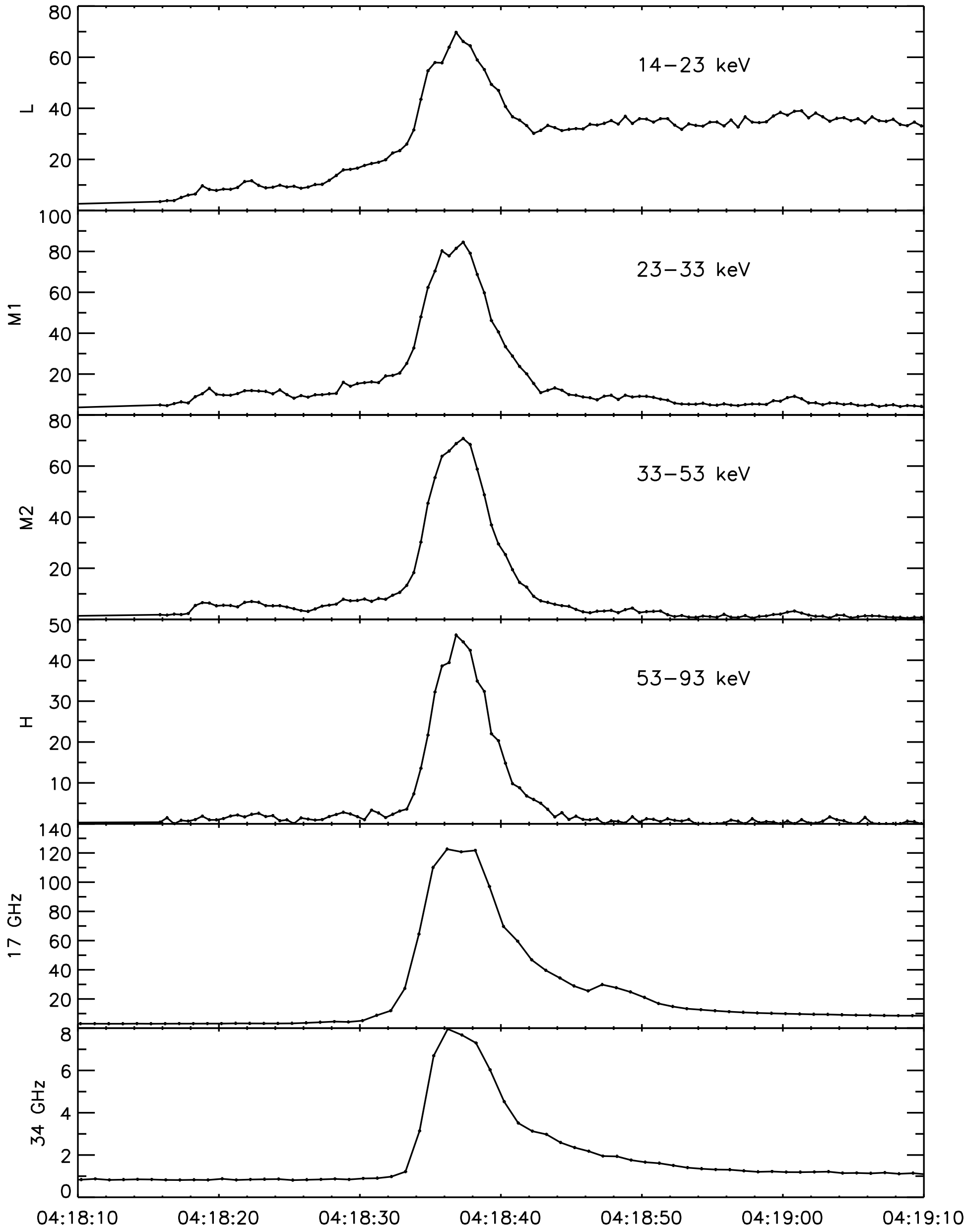

Fig. 4.— Time profiles of the hard X–ray emission in 4 channels (the top four panels are the H, M2, M1, and L bands, respectively) as observed by Yohkoh/HXT, along with NoRH 17 GHz and 34 GHz time profiles (bottom two panels) for the simple spiky burst of June 13, 1998.

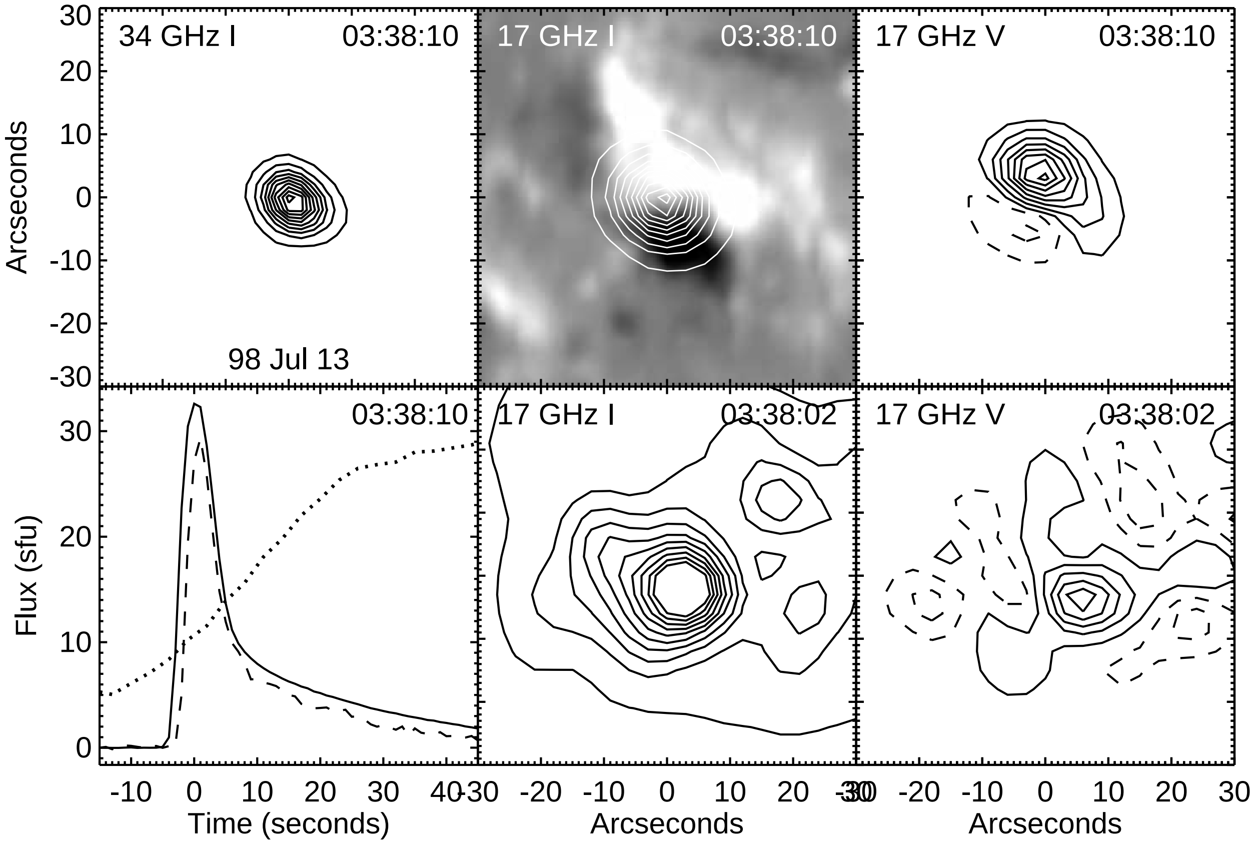

Fig. 5.— NoRH time profiles and images of the flare at 03:38:10 UT on 1998 July 13. The format is identical to that of Fig. 1, with the peak brightness temperatures being 5.2×10^6 K at 34 GHz and 1.2×10^7 K at 17 GHz. In the preflare images, contours are plotted at brightness temperatures of 15000, 25000, ..., 105000 K in the total intensity map and ±2500, ±7500, ..., ±22500 K in the circularly polarized map. The magnetogram in this figure is from the Kitt Peak National Observatory spectromagnetograph, acquired at about 14:06 UT on the previous day and shown rotated to the time of the flare.

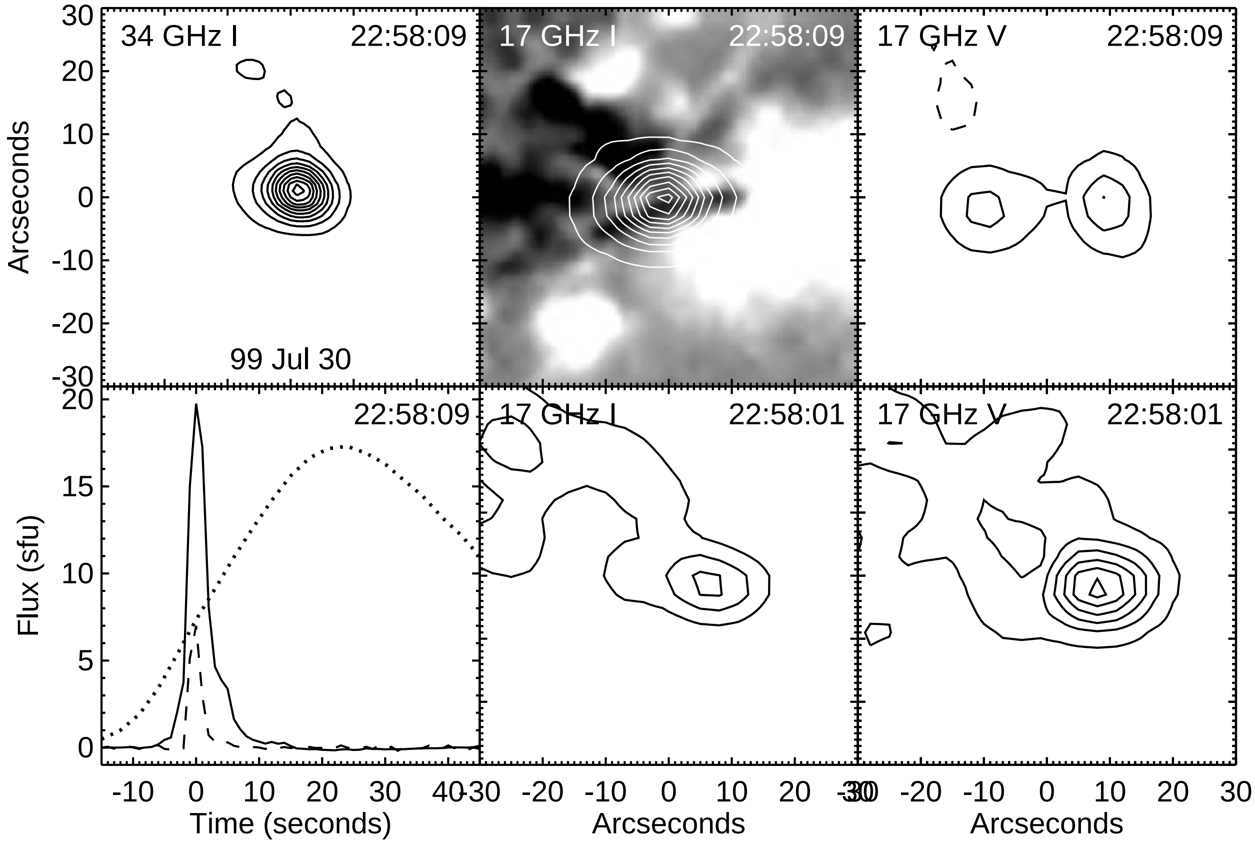

Fig. 6.— NoRH time profiles and images of the flare at 22:58:09 UT on 1999 July 30. The format is identical to that of Fig. 1, with the peak brightness temperatures being 2.4 $\times$ 10^6 K at 34 GHz and 6.5 $\times$ 10^6 K at 17 GHz. In the preflare images, contours are plotted at brightness temperatures of 75000, 125000, ..., 425000 K in the total intensity map and $\pm$12500, $\pm$37500, ..., $\pm$237500 K in the circularly polarized map. The SOHO/MDI magnetogram was taken at 22:24:02 UT.

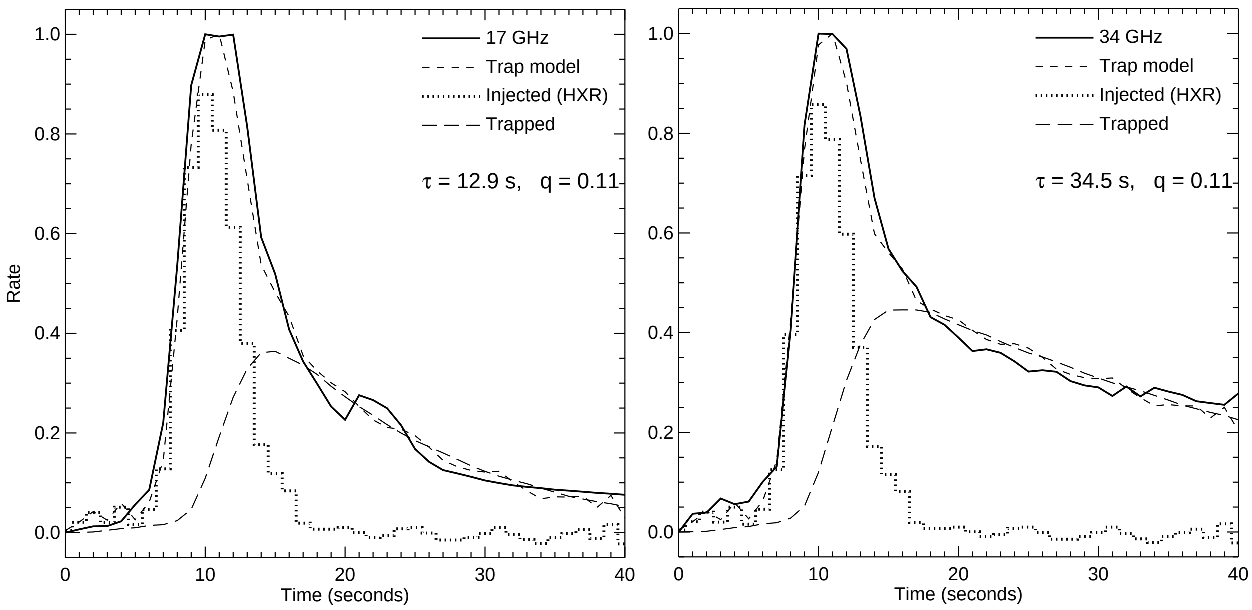

Fig. 7.— Comparison of the radio time profiles for the event on 1998 June 13 (left panel: 17 GHz; right panel: 34 GHz) with a trap model (short dashed line) derived using the *Yohkoh*/HXT 53 – 93 keV hard X-ray time profile shown as a dotted histogram) as an injection function. The radio time profile is modelled as the sum of a component identical to the hard X–ray time profile (the injection function) and a trapped component (long dashed line) derived by integrating over the injection function convolved with an exponential decay term (time constant τ). All time profiles are normalized to a peak of unity and the parameter q specifies the relative contributions of the injected and trapped components (see text).

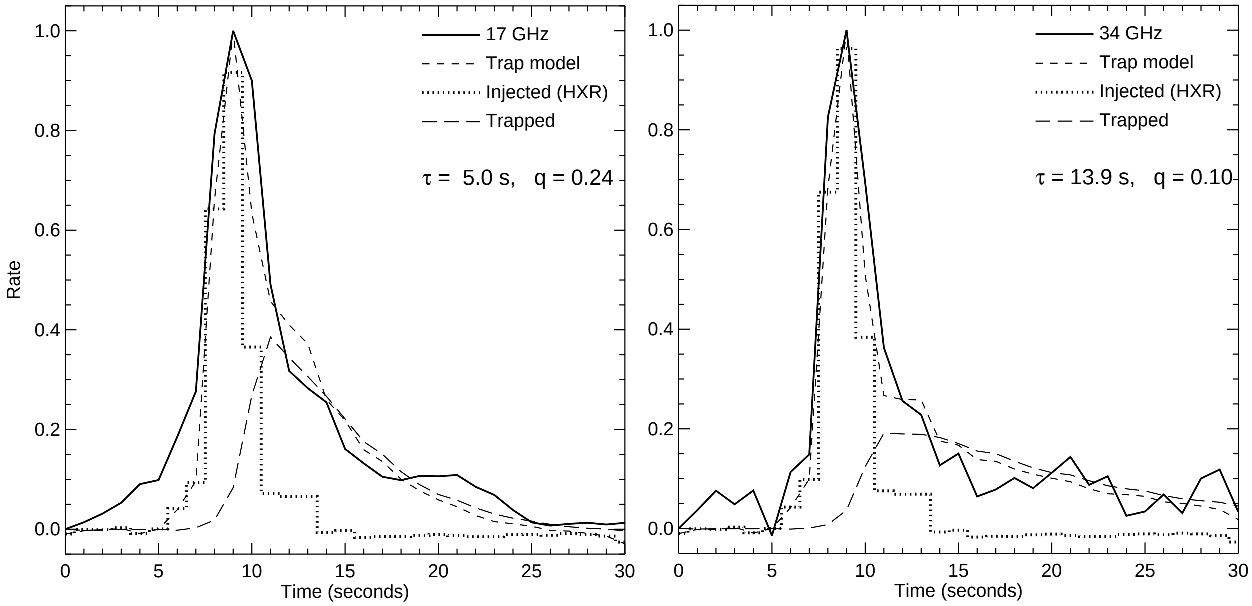

Fig. 8.— Comparison of the radio time profiles for the event on 1999 July 30 (left panel: 17 GHz; right panel: 34 GHz) with a trap model using the same format as in Figure 7. In this case the injection function is taken from the 50 – 100 keV measurements of the *CGRO*/BATSE detectors.